photonics

MDPI

Communication

All-Fiber Gas Raman Laser by D_2-Filled Hollow-Core Photonic Crystal Fibers

Wenxi Pei [1,2], Hao Li [1,3], Wei Huang [1,3], Meng Wang [1,2,3] and Zefeng Wang [1,2,3,*]

[1] College of Advanced Interdisciplinary Studies, National University of Defense Technology, Changsha 410073, China; peiwenxi@nudt.edu.cn (W.P.); lihao18c@nudt.edu.cn (H.L.); huangw2684@nudt.edu.cn (W.H.); wangmeng@nudt.edu.cn (M.W.)
[2] Hunan Provincial Key Laboratory of High Energy Laser Technology, Changsha 410073, China
[3] State Key Laboratory of Pulsed Power Laser Technology, Changsha 410073, China
* Correspondence: zefengwang@nudt.edu.cn

Abstract: We report here an all-fiber structure tunable gas Raman laser based on deuterium-filled hollow-core photonic crystal fibers (HC-PCFs). An all-fiber gas cavity is fabricated by fusion splicing a 49 m high-pressure deuterium-filled HC-PCF with two solid-core single-mode fibers at both ends. When pumped with a pulsed fiber amplifier seeded by a tunable laser diode at 1.5 μm, Raman lasers ranging from 1643 nm to 1656 nm are generated. The maximum output power is ~1.2 W with a Raman conversion efficiency of ~45.6% inside the cavity. This work offers an alternative choice for all-fiber lasers operating at 1.6–1.7 μm band.

Keywords: photonic crystal fibers; hollow-core fibers; fiber lasers; stimulated Raman scattering; gas Raman lasers

Citation: Pei, W.; Li, H.; Huang, W.; Wang, M.; Wang, Z. All-Fiber Gas Raman Laser by D_2-Filled Hollow-Core Photonic Crystal Fibers. *Photonics* **2021**, *8*, 382. https://doi.org/10.3390/photonics8090382

Received: 18 August 2021
Accepted: 6 September 2021
Published: 9 September 2021

1. Introduction

Stimulated Raman scattering (SRS) of gas medium has received great attention since it was first reported [1]. It provides a novel way to generate lasers with unobtainable wavelength for traditional schemes, especially in the ultraviolet and infrared spectral range. However, due to the short reaction length and weak reaction intensity, gas Raman lasers based on the traditional gas cell usually require high pump power, and the corresponding conversion is always inefficient. Moreover, there is often more than one Raman line at the output except the desired line, which exacerbates the inefficiency. The advent of the hollow-core fibers (HCFs) provides new opportunities for efficient gas SRS [2,3]. This kind of innovative gas cell based on HCFs can provide a much longer reaction distance, and the pump laser and gas molecules are confined in the micron-level air core, which enhances the reaction intensity greatly. More importantly, the HCF makes it easy to control the transmission spectrum by designing fiber structure, so the conversion of unwanted Raman lines can be well suppressed, which further improves the conversion efficiency. Therefore, fiber gas Raman lasers (FGRLs) have drawn great attention with the fast development of the HCFs [4–7].

Fiber lasers operating at 1.6~1.7 μm band have been studied extensively, owing to their significant applications [8]. They play a great role in medical treatment [9,10], material processing [11], the generation of mid-infrared lasers [12] and so on. Several approaches for generating the laser at this band have been reported, which can be divided into two categories. One is based on the rare-earth doped fibers, such as thulium-doped fibers (TDFs) and bismuth-doped fibers (BDFs), which is mainly limited by the low gain of the fiber in this band or immature manufacturing technology. The other is to take advantage of nonlinear effects based on SRS in the solid-core fibers, while the complex cascade structure is always necessary. The advent of fiber gas lasers based on SRS provides a novel method for the generation of laser emission at some wavelengths not easily achievable with

traditional ways, including 1.6–1.7 μm band [13–17]. By using proper HCFs and proper active gas medium, laser emissions can be realized flexibly and effectively. Moreover, due to the higher damage threshold of the HCF, it is more possible for FGRLs to realize higher output power. Recently, we have reported some works on 1.6–1.7 μm gas-filled FGRLs [13–18]. The common gas media used in our work are hydrogen and deuterium. Compared with hydrogen, D_2 has a larger molecular weight, making it easier to confine it inside the HCF. Besides, D_2 has a much smaller coefficient of Raman shift, which generates and enriches the unobtainable laser wavelength in this band. In our previous work, we demonstrated a subwatt 1.65 μm FGRL based on D_2-filled hollow-core photonic crystal fibers (HC-PCFs) [16], and then further improved its output power [17]. However, both of them sealed the output end in a customized gas chamber, making the system bulky and poorly stabilized, which limits its application in the future.

Here, we report a 1.65 μm all-fiber tunable pulsed FGRL based on D_2-filled HC-PCFs. The all-fiber gas cavity is fabricated by fusion splicing a 49 m high-pressure deuterium-filled HC-PCF with two solid-core single-mode fibers at both ends. When pumped by a homemade fiber amplifier at 1.5 μm band, the pure rotational SRS occurs in the gas cavity, generating first-order Raman lasers ranging from 1643 nm to 1656 nm. The maximum output Raman power of ~1.2 W at 1645 nm is obtained with the repetition frequency of 2.2 MHz when pump power is at the maximum. The Raman conversion efficiency inside the cavity is ~45.6%. This work enriches the research on FGRLs and provides a convenient choice for generation of fiber lasers operating at the 1.6–1.7 μm band.

2. Experimental Setup

Figure 1a shows the schematic diagram of experimental setup, which is similar to our previous work [15], but a longer HC-PCF is introduced. A homemade narrow-linewidth pulsed Erbium-doped fiber amplifier (EDFA) seeded by a tunable laser diode at 1.5 μm works as the pump source. The width of the output pulse is 20 ns and it remains the same when the repetition frequency or output power changes. The repetition frequency is adjustable, and the power characteristics are basically the same, with the pulse width of 20 ns in different repetition frequency. The pump source can be tuned in the range of 1538 nm to 1545 nm, which retains the similar characteristics when the wavelength changes. Figure 1b–d show the output spectrum of the EDFA with different operating wavelengths when the output power is the maximum of ~7 W. It can be seen that although the amplified spontaneous emission is generated during the amplification, it can always be well suppressed. An ultra-low-loss fiber coupler with the measured coupling ratio of 99.06:0.94 is spliced to the pigtail of the EDFA to monitor the real output power. Its signal end is spliced to the port1 of a circulator, which is introduced to protect the pump source and measure backward light at port3, as marked in the figure. The loss of the circulator from port1 to port2 is ~0.67 dB. An all-fiber gas cavity is fabricated by a 49 m long HC-PCF (HC-1550-02, NKT Photonics) and two solid-core single-mode fibers (SMF-28e, Corning), as shown within the dashed box in Figure 1a. One of the solid-core fibers is employed to be the input end of the cavity, which is spliced with the circulator port2 and one end of the HC-PCFs, respectively. After being vacuumized, the HC-PCF is inflated with high-pressure D_2 and stands until the gas pressure is balanced. Then the other end that was sealed in the gas chamber is spliced to another solid-core fiber, which works as the output end of the gas cavity. The final gas pressure in the cavity is estimated to be 25.5 bar by calculating the time and gas leakage ratio. The core diameter of the HC-PCFs is 10 μm and its cross section by optical microscope is shown in Figure 1e. Due to the similar mode field diameter (~9 μm) of SMF-28e and HC-1550-02, the loss of fusion splicing directly is acceptable. The losses of the fusion splicing points marked as splice1 and splice2 are 1.4 dB and 2 dB, respectively. Two lenses with the focal length of 15 mm are placed at the output end of the gas cavity and the circulator port3 separately to collimate the output beam. Two long-pass filters (transmission ~95% > 1600 nm) play the role of separating the pump light and Raman light.

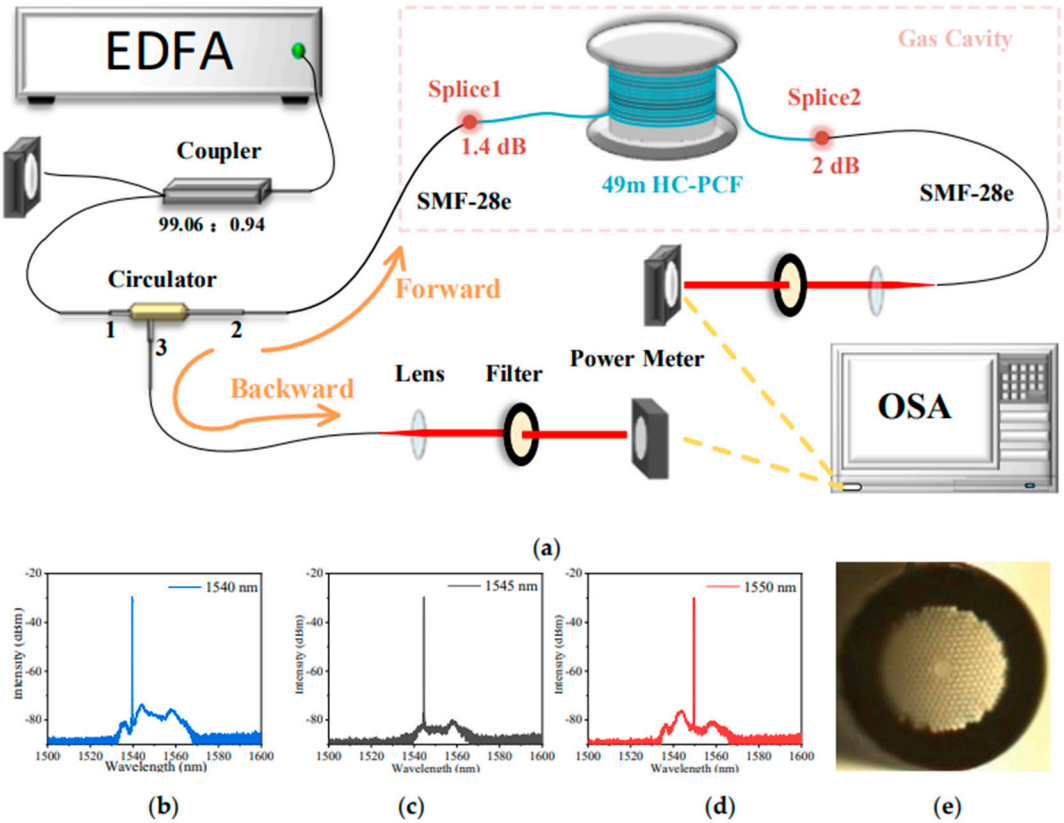

Figure 1. (**a**) The schematic diagram of experimental setup. OSA: optical spectrum analyzer. EDFA: Erbium-doped fiber amplifier; (**b**–**d**) the output spectrum of the EDFA at the maximum output power; (**e**) the cross section of the used HC-PCFs by optical microscope.

3. Results and Discussion

3.1. Spectrum Characteristics

Figure 2a shows the measured output spectrum with different pump wavelengths when the pump source works at the maximum output power. The repetition frequency (RF) is set to 4 MHz. When pumped by the lines at 1538 nm to 1550 nm, the pure rotational SRS of D_2 occurs in the cavity, generating Raman lines ranging from 1643 nm to 1656 nm with the Raman shift of ~414 cm^{-1}. Each pump line corresponds to only one Raman line. Figure 2b shows the fine spectrum of the Raman line at 1645 nm (in red line) and the pump line at 1540 nm (in blue dotted line), respectively. It can be seen that the central wavelength of the pump line is at 1539.9 nm. For ease of expression and readability of the paper, we express it as 1540 nm.

Figure 3a presents the measured transmission spectrum of the HC-PCF, covering 1530 nm to 1760 nm. When the pump wavelength is set to 1540 nm, we measured the output spectrum with different RF at the maximum output power, as shown in Figure 3b–f. It can be seen in Figure 3b that when the RF is 1 MHz, due to the high peak power, more than one Raman line occurs in the gas cavity. In addition to the pump line at 1540 nm and the first-order Raman line at 1645 nm, there are 3 s order Raman lines. The lines at 1695 nm, 1730 nm and 1765 nm correspond to the frequency shift of ~179 cm^{-1}, ~298 cm^{-1} and ~414 cm^{-1}, respectively. High peak power of the pump pulse is more likely to exceed the high-order Raman threshold, leading to the cascaded Raman conversion. The output power of the first-order Raman laser and its conversion efficiency may be reduced in this case. Compared with H_2, D_2 has a much smaller coefficient of Raman shift, permitting the existence of some high-order Raman lines in the transmission band of the HC-PCF. It not

only enriches the output wavelength in 1.7 μm band, but also makes it possible to realize the cascade Raman laser output if the fiber Bragg granting is introduced.

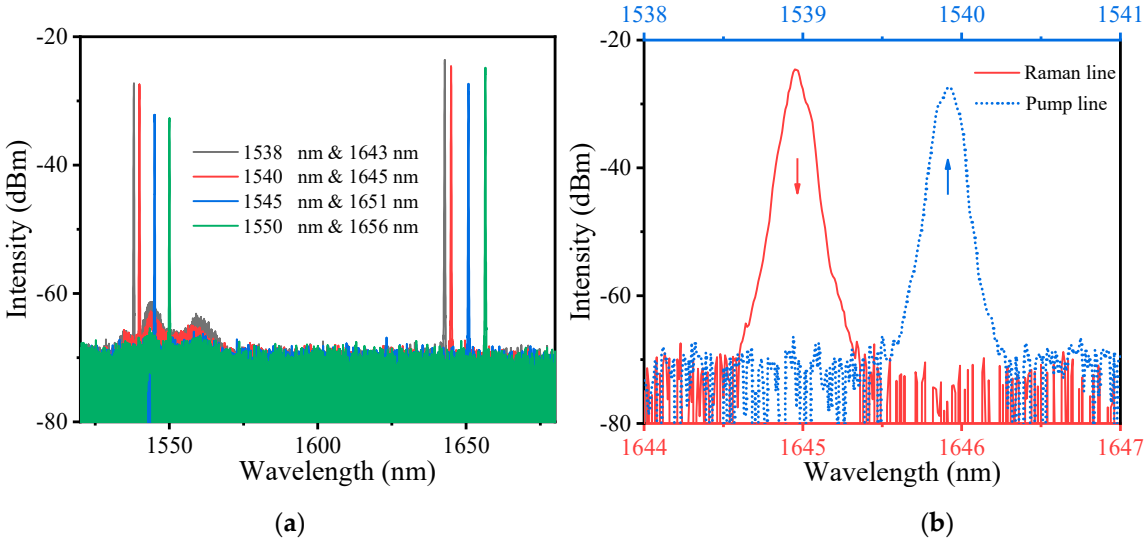

Figure 2. (**a**) The output spectrum of the fiber gas Raman laser pumped by different pump wavelengths at the maximum output power. (**b**) The fine spectrum of the Raman lines at 1645 nm (in red line) and the pump lines at 1540 nm (in blue dotted line).

When the RF is 2 MHz in Figure 3c, besides the pump lines and the first-order Raman lines, there is only a weak second-order Raman line at 1765 nm due to the reduction of the pulse peak power. It also indicates that for D_2 inside the gas cavity, the rotational SRS whose Raman shift is ~414 cm^{-1} corresponds to the stronger Raman gain (both the frequency shifts of these two Raman lines are ~414 cm^{-1}).

Interestingly, when the RF is set to 3 MHz in Figure 3d, there are two second-order Raman lines at 1695 nm and 1730 nm again. This can be explained by the following theory. For the gas cavity, we regard it as a special resonant cavity formed by the 49 m HC-PCFs and two fusion splicing points (splice1 and splice2). Its average refractive index is ~1, so the resonant frequency can be calculated through the formula: $v_p = qc/2L$, where v_p is the resonant frequency, q is a positive integer (the number of the pulse round trip through the cavity), c is the speed of light ($2.997*10^8$ m/s) and L is the length of resonant cavity. In our work, L is 49 m; then the v_p can be calculated to be ~3 MHz when the q is 1. For the pump pulse RF of 3 MHz, it is consistent with the resonant frequency. While the pump pulses oscillate in the cavity, they can coincide with previous pulses, which means that the resonant cavity can provide positive feedback to reduce the Raman threshold and benefit the conversion. Therefore, there are still high-order Raman lines in this case. The absence of the line at 1765 nm is mainly due to the high transmission loss and the lower peak power. Furthermore, the specific Raman threshold power has been measured, as discussed in the following Section 3.2. Power Characteristics, which also supports this theory.

As we can see in Figure 3e,f, there are no high-order lines when the RFs are 4 MHz and 5 MHz, which is due to the continuous decrease of the peak power. It should be noted that when the RF is 5 MHz, the intensity of the first-order Raman line at 1645 nm is 3.065 dB weaker than that of the pump line at 1540 nm, which indicates the insufficient conversion in the gas cavity.

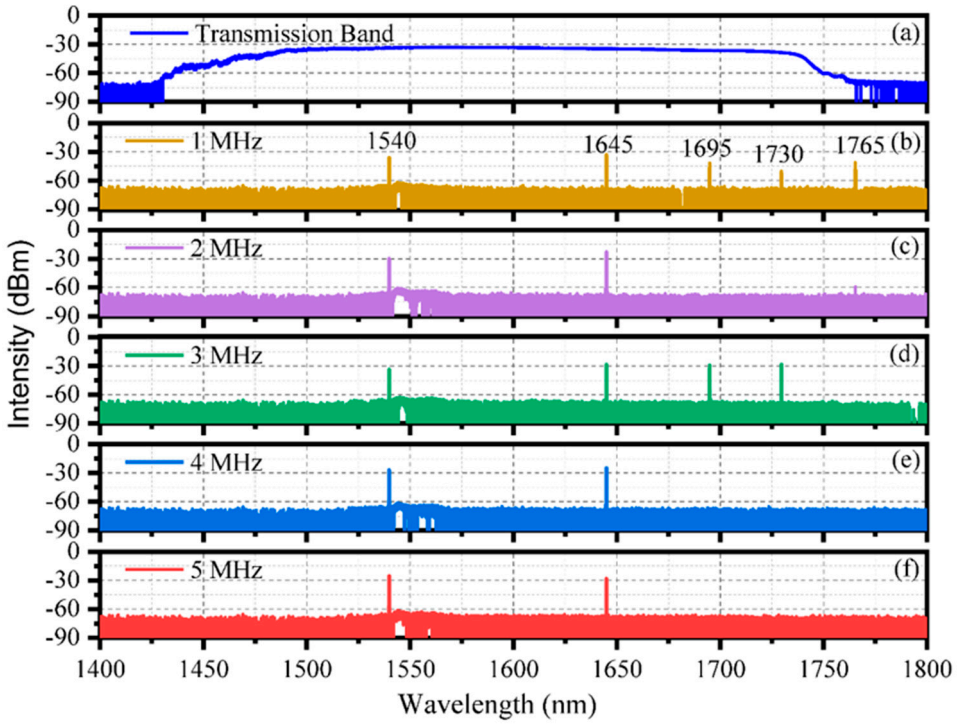

Figure 3. (**a**) The measured transmission spectrum of the HC-PCF. (**b**–**f**) The output spectrum of the fiber gas Raman laser pumped by the pulse with different RF at the maximum output power.

3.2. Power Characteristics

To explore the maximum output power and the corresponding conversion efficiency of the first-order Raman laser at 1645 nm, we measured the power characteristics with the RF of 2 MHz, 4 MHz and 5 MHz, as shown in Figure 4. All the powers in the figure are the average powers of the pulse train. The power characteristics with the RF of 1 MHz or 3 MHz are not measured due to their complex spectrum characteristics (as shown in Figure 3), which have multi-wavelength output at the maximum pump power and cannot separate the unwanted lines easily. The incident pump power is the output power of the circulator port2. Figure 4a,b show the characteristics of forward Raman power and pump power. It can be seen that the Raman threshold average power with the RF of 2 MHz is much lower than that of the RF in 4 MHz and 5 MHz, as the peak power of pump pulse in 2 MHz is much higher. When the incident pump power exceeds threshold power, all the curves of the pump power drop and Raman power increases gradually. The maximum forward Raman power of ~1.13 W is achieved at the maximum pump power when the RF is 2 MHz. Figure 4c presents the backward Raman power characteristics. Obviously, backward Raman power is much lower than forward Raman power, as it is reflected by the splice2. We calculated the ratio of the maximum backward Raman power to the maximum forward Raman power; the value is ~3.28%, ~15.94% and ~16.92% when the corresponding RF is 2 MHz, 4 MHz and 5MHz, respectively. This indicates that the high RF is conductive to the amplification of the backward Raman power. The curves of backward pump power in Figure 4d are basically the same, and the reason is that they are incident pump power that is reflected by the splice1. All the pump powers in Figure 4d keep increasing as the incident pump power increases.

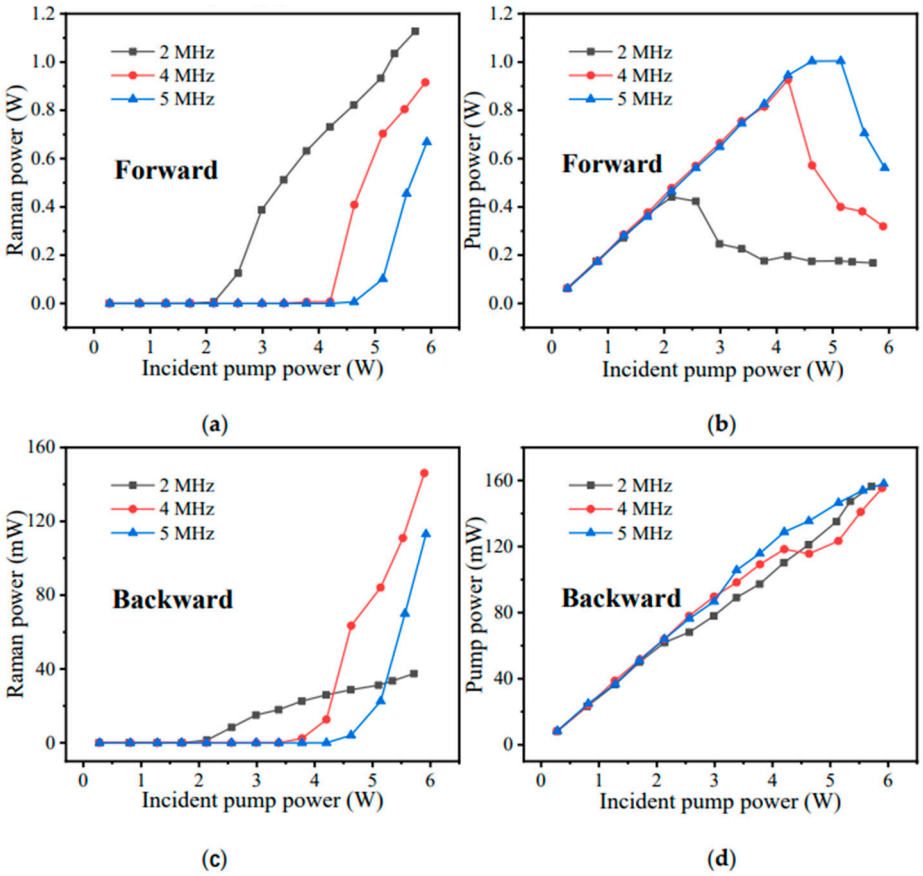

Figure 4. The output power characteristics of the fiber gas Raman laser with the repetition frequency of 2 MHz, 4 MHz and 5 MHz: (**a**) forward Raman power; (**b**) forward pump power; (**c**) backward Raman power; (**d**) backward pump power.

Figure 5a shows the evolution of the Raman threshold average power and peak power with different RF of the pump pulse. Here we define the Raman threshold power as the minimum pump power coupled in the HC-PCF when the first-order Raman laser can be detected by the OSA at the output end of the cavity. We measured the Raman threshold power with the RF from 1 MHz to 5 MHz; it can be seen that except for the case with the RF of 3 MHz, all the peak power of the Raman threshold is basically the same and the Raman threshold average power increases with the increasing of the RF. This is not unexpected, because the peak power of the Raman threshold is constant for a certain cavity, which is mainly determined by the gas pressure inside the cavity or the length of the HC-PCF. However, when the RF of 3 MHz is consistent with the resonant frequency mentioned above, the positive feedback caused by the cavity and the coincidence between pulses greatly reduce the peak power of the Raman threshold. Therefore, its threshold characteristics differ from those of the other RF, meaning that there may be high-order Raman laser when the pump power increases in this case, as discussed above. Furthermore, we also measured the threshold power with the RF of 6 MHz, which is another resonant frequency of the cavity (the corresponding q is 2), as shown in Figure 5a. It can be seen that its peak power of the Raman threshold is the same as that of 3 MHz, but the Raman threshold average power is double, which is because the RF of 6 MHz is the double of 3 MHz. This confirms the conclusion and provides a new way for realizing multi-wavelength FGRL with all-fiber structure. Moreover, we calculated the total Raman power and internal Raman power (Raman power inside the gas cavity) with different RF when the pump power is at the maximum, as shown in Figure 5b. The Raman power at 1645 nm with RF of 1 MHz or 3 MHz is not obtained because of the existence of the high-order Raman power with low-threshold characteristic. Obviously, the maximum Raman power

can be achieved when the RF is 2 MHz. The total Raman power is ~1.16 W, and the internal Raman power is calculated to be 1.85 W, which is much higher than that with other RF.

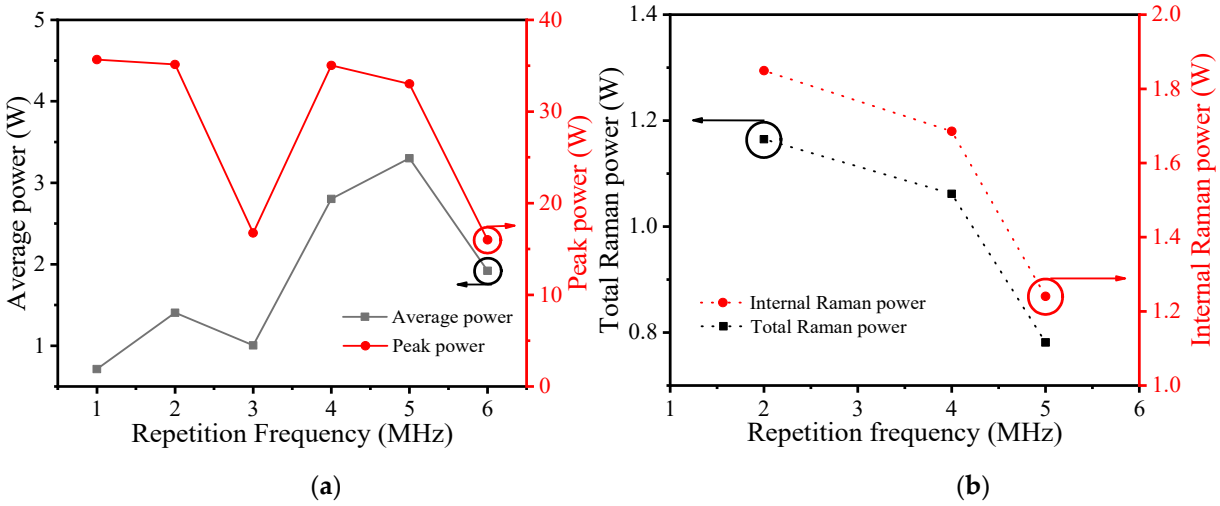

Figure 5. (**a**) The evolution of the Raman threshold average power and the corresponding peak power with repetition frequency ranging from 1 MHz to 6 MHz. (**b**) The variation of total Raman power and the corresponding internal Raman power inside the HC-PCF with the repetition frequency when the pump power is the maximum.

Then, we changed the RF in steps of 200 kHz and measured their Raman power characteristics, as shown in Figure 6. As shown in Figure 6a,b, both the maximums of forward and backward Raman power are achieved at the maximum pump power when the RF is set to 2.2 MHz. When the RF is 1.6 MHz and 1.8 MHz, the corresponding Raman powers increase at first, but decrease later when the incident pump power is high enough. This is mainly because the peak power of the pump pulse with these RF is higher than that of the other RF, and the first-order Raman laser is converted into high-order Raman laser when its power is high enough. However, due to the high transmission loss, the power of the high-order Raman laser is exhausted and cannot be measured. Figure 6c shows the evolution of the total and internal Raman power with different RF when the pump power is at the maximum, respectively. The maximum total Raman power of ~1.2 W is obtained when the RF is 2.2 MHz, and the corresponding internal Raman power is ~1.9 W. Its optical–optical conversion efficiency is ~21.2% and the corresponding conversion efficiency inside the cavity is ~45.6%. By contrast, the power with the RF of 1.6 MHz and 1.8 MHz is much lower than that with other RF, which is mainly due to the high-order Raman conversion. Figure 6d presents the maximum optical–optical conversion efficiency with different RF. The efficiency inside the gas cavity without the loss caused by splice1 and splice2 is also calculated. This shows that the maximum of total conversion efficiency is above 20% with different RF, but when the splice loss is considered, the efficiency is more than 40%. It enlightens us that if the splice loss of the gas cavity can be optimized, the conversion efficiency can be further improved.

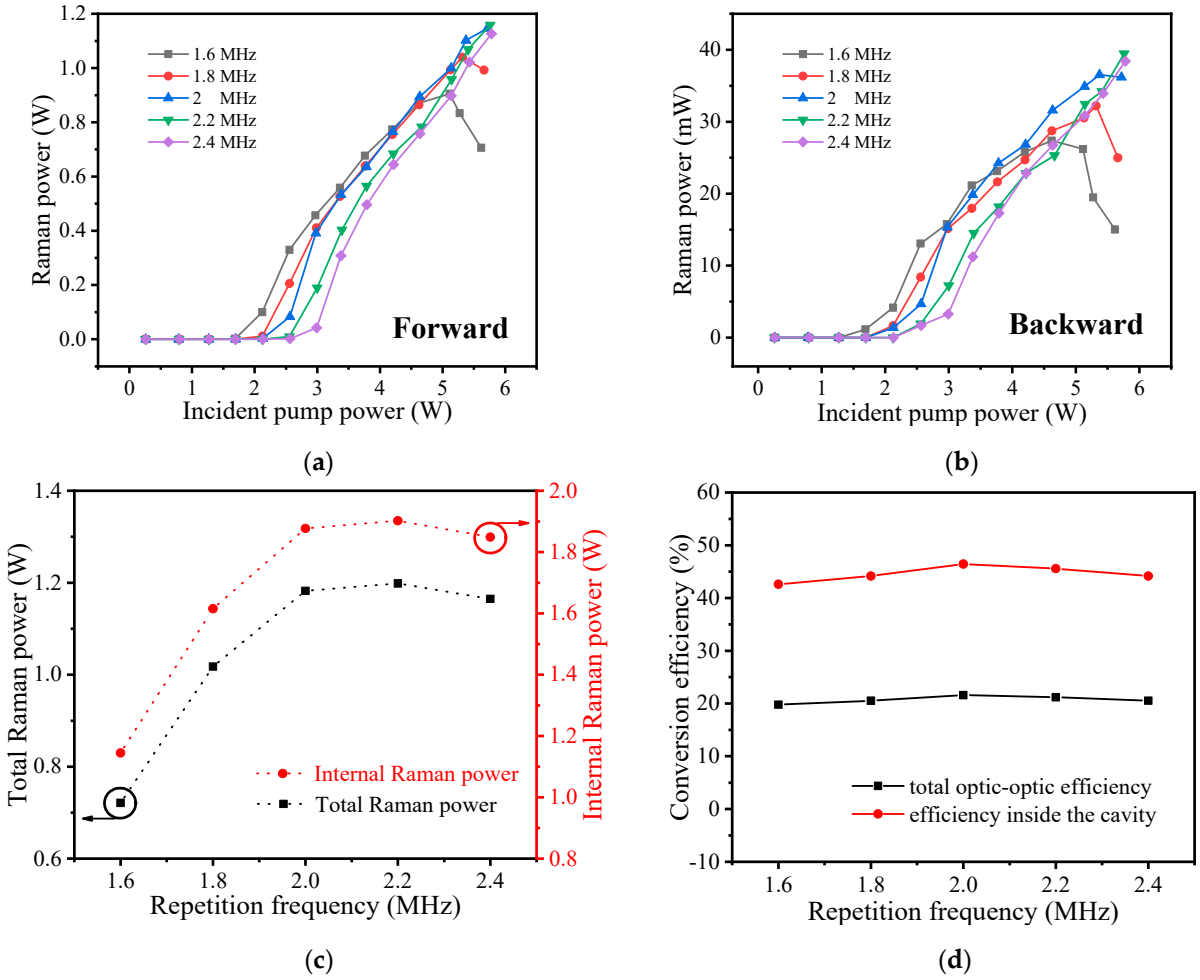

Figure 6. The output power characteristics of the fiber gas Raman laser with the repetition frequency of 1.6 MHz to 2.4 MHz: (**a**) forward Raman power; (**b**) backward Raman power; (**c**) the evolution of the total and internal Raman power with different repetition frequency when the pump power is at the maximum; (**d**) the evolution of the maximum conversion efficiency with different repetition frequency.

3.3. Pulse Shapes

Figure 7 shows the shapes of output pulse when the maximum is obtained with the pulse RF of 2.2 MHz. A bandpass filter (1530–1570 nm) and a long-pass filter (transmission ~95% > 1600 nm) are used for separating pump pulse and Raman pulse. The pulse can be detected by a fast photodetector (EOT ET5000) and a broadband oscilloscope (Tektronix MDO3104). It can be seen from Figure 7a that the shape of the residual forward pump pulse has a dip in the middle. The reason is that for a pump pulse in the cavity, only the part with higher energy can exceed the Raman threshold power and be converted into the Raman pulse, which results in the dip at its middle part. Thereby, the width of the Raman pulse is close to that of the dip, which is narrower than the pump pulse. Backward pulse shapes in Figure 7b differ from those of the forward pulse. It can be seen that pump pulse and Raman pulse are not caught at the same time, and there is a ~330 ns time delay. As analyzed above, the backward Raman pulse is reflected by the splice2, which has quite a low power, leading to the weak intensity of the measured pulse shape. The transmission length of the backward Raman pulse is double the length of the gas cavity (~100 m), which causes the time delay of ~330 ns.

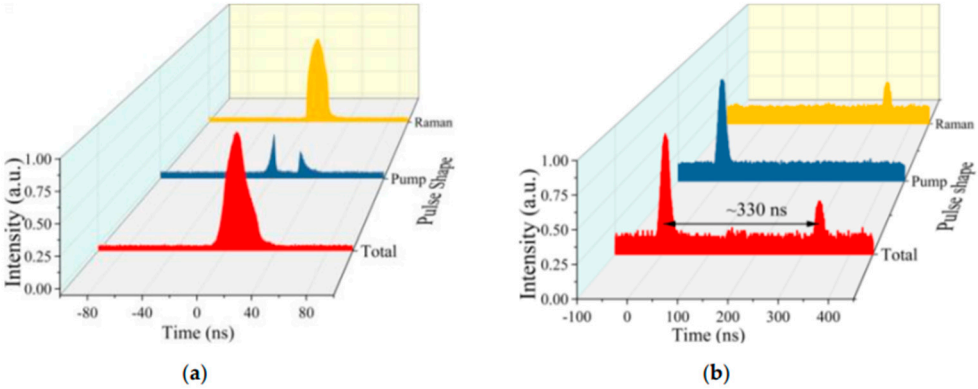

Figure 7. The output pulse shapes of the fiber gas Raman laser with the repetition frequency of 2.2 MHz at the maximum pump power: (**a**) forward output pulse; (**b**) backward output pulse.

4. Conclusions

We have demonstrated a 1.65 μm all-fiber tunable FGRL based on the pure rotational SRS in the D_2.-filled HC-PCFs. An all-fiber gas cavity is realized by a 49 m long HC-PCF and two solid-core fibers. Pumped by a 1.5 μm homemade pulsed EDFA, 1643 nm to 1656 nm Raman laser is generated in the gas cavity. The maximum output power of ~1.2 W at 1645 nm is obtained when the pump laser is at 1540 nm. The efficiency inside the cavity is ~45.6%; however, the corresponding total conversion efficiency is only 21.2% due to the relative high splicing loss at present, which could be greatly reduced by more precise mode field matching methods [19,20]. This work provides a convenient alternative choice for generation of fiber lasers operating at 1.6–1.7 μm band. By optimizing the length of HC-PCF and reducing the loss of the splicing point, the conversion efficiency and output laser power could be greatly improved.

Author Contributions: Conceptualization, Z.W. and W.P.; methodology, W.P.; software, W.H. and H.L.; validation, Z.W., H.L., W.H. and W.P.; formal analysis, Z.W. and H.L.; investigation, W.P.; resources, M.W. and W.P.; data curation, H.L.; writing—original draft preparation, W.P.; writing—review and editing, Z.W.; visualization, W.P. All authors have read and agreed to the published version of the manuscript.

Funding: This work was supported by the Outstanding Youth Science Fund Project of Hunan Province Natural Science Foundation (2019JJ20023), National Natural Science Foundation of China (NSFC) (11974427, 12004431), and State Key Laboratory of Pulsed Power Laser Technology (SKL2020ZR05, SKL2021ZR01).

Data Availability Statement: The data presented in this study are available on request from the corresponding author. The data are not publicly available due to privacy.

Conflicts of Interest: The authors declare no conflict of interest.

References

1. Minck, R.W.; Terhune, R.W.; Rado, W.G. Laser-stimulated Raman Effect and Resonant Four-photon Interactions in gases H_2, D_2, and CH_4. *Appl. Phys. Lett.* **1963**, *3*, 181–184. [CrossRef]
2. Cregan, R.F. Single-Mode Photonic Band Gap Guidance of Light in Air. *Science* **1999**, *285*, 1537–1539. [CrossRef] [PubMed]
3. Benabid, F.; Knight, J.C.; Antonopoulos, G.; Russell, P.S.J. Stimulated Raman Scattering in Hydrogen-Filled Hollow-Core Photonic Crystal Fiber. *Science* **2002**, *298*, 399–402. [CrossRef] [PubMed]
4. Benabid, F.; Bouwmans, G.; Knight, J.C.; Russell, P.S.J.; Couny, F. Ultrahigh Efficiency Laser Wavelength Conversion in a Gas-Filled Hollow Core Photonic Crystal Fiber by Pure Stimulated Rotational Raman Scattering in Molecular Hydrogen. *Phys. Rev. Lett.* **2004**, *93*, 123903. [CrossRef] [PubMed]
5. Couny, F.; Benabid, F.; Light, P.S. Subwatt Threshold Cw Raman Fiber-Gas Laser Based on H_2 -Filled Hollow-Core Photonic Crystal Fiber. *Phys. Rev. Lett.* **2007**, *99*, 143903. [CrossRef] [PubMed]
6. Wang, Z.; Yu, F.; Wadsworth, W.J.; Knight, J.C. Efficient 1.9 μm Emission in H_2-Filled Hollow Core Fiber by Pure Stimulated Vibrational Raman Scattering. *Laser Phys. Lett.* **2014**, *11*, 105807. [CrossRef]

7. Li, Z.; Huang, W.; Cui, Y.; Wang, Z. Efficient Mid-Infrared Cascade Raman Source in Methane-Filled Hollow-Core Fibers Operating at 2.8 μm. *Opt. Lett.* **2018**, *43*, 4671. [CrossRef] [PubMed]
8. Zhang, Y.; Zhang, P.; Liu, P.; Han, K.; Du, Q.; Wang, T.; Zhang, L.; Tong, S.; Jiang, H. Fiber Light Source at 1.7 μm Waveband and Its Applications. *Laser Optoelectron. Prog.* **2016**, *53*, 090002. [CrossRef]
9. Piao, Z.; Ma, T.; Li, J.; Wiedmann, M.T.; Huang, S.; Yu, M.; Kirk Shung, K.; Zhou, Q.; Kim, C.-S.; Chen, Z. High Speed Intravascular Photoacoustic Imaging with Fast Optical Parametric Oscillator Laser at 1.7 Mm. *Appl. Phys. Lett.* **2015**, *107*, 083701. [CrossRef] [PubMed]
10. Alexander, V.V.; Ke, K.; Xu, Z.; Islam, M.N.; Freeman, M.J.; Pitt, B.; Welsh, M.J.; Orringer, J.S. Photothermolysis of Sebaceous Glands in Human Skin Ex Vivo with a 1708 nm Raman Fiber Laser and Contact Cooling: PHOTOTHERMOLYSIS OF SEBACEOUS GLANDS. *Lasers Surg. Med.* **2011**, *43*, 470–480. [CrossRef] [PubMed]
11. Mingareev, I.; Weirauch, F.; Olowinsky, A.; Shah, L.; Kadwani, P.; Richardson, M. Welding of Polymers Using a 2 μm Thulium Fiber Laser. *Opt. Laser Technol.* **2012**, *44*, 2095–2099. [CrossRef]
12. Quimby, R.S.; Shaw, L.B.; Sanghera, J.S.; Aggarwal, I.D. Modeling of Cascade Lasing in Dy: Chalcogenide Glass Fiber Laser with Efficient Output at 4.5 μm. IEEE Photon. *Technol. Lett.* **2008**, *20*, 123–125. [CrossRef]
13. Huang, W.; Li, Z.; Cui, Y.; Zhou, Z.; Wang, Z. Efficient, Watt-Level, Tunable 1.7 μm Fiber Raman Laser in H_2-Filled Hollow-Core Fibers. *Opt. Lett.* **2020**, *45*, 475–478. [CrossRef]
14. Li, H.; Pei, W.; Huang, W.; Wang, M.; Wang, Z. Highly Efficient Nanosecond 1.7 μm Fiber Gas Raman Laser by H_2-Filled Hollow-Core Photonic Crystal Fibers. *Crystals* **2020**, *11*, 32. [CrossRef]
15. Pei, W.; Li, H.; Huang, W.; Wang, M.; Wang, Z. All-Fiber Tunable Pulsed 1.7 μm Fiber Lasers Based on Stimulated Raman Scattering of Hydrogen Molecules in Hollow-Core Fibers. *Molecules* **2021**, *26*, 4561. [CrossRef] [PubMed]
16. Cui, Y.; Huang, W.; Li, Z.; Zhou, Z.; Wang, Z. High-Efficiency Laser Wavelength Conversion in Deuterium-Filled Hollow-Core Photonic Crystal Fiber by Rotational Stimulated Raman Scattering. *Opt. Express* **2019**, *27*, 30396. [CrossRef] [PubMed]
17. Li, H.; Huang, W.; Cui, Y.; Zhou, Z.; Wang, Z. 3 W Tunable 1.65 μm Fiber Gas Raman Laser in D_2-Filled Hollow-Core Photonic Crystal Fibers. *Opt. Laser Technol.* **2020**, *132*, 106474. [CrossRef]
18. Li, H.; Huang, W.; Cui, Y.; Zhou, Z.; Wang, Z. Pure rotational stimulated Raman scattering in H_2-filled hollow-core photonic crystal fibers. *Opt. Express* **2020**, *28*, 23881. [CrossRef] [PubMed]
19. Yu, R.; Wang, C.; Benabid, F.; Chiang, K.; Xiao, L. Robust mode matching between structurally dissimilar optical fiber waveguides. *ACS Photonics* **2021**, *8*, 857. [CrossRef]
20. Wang, C.; Yu, R.; Debord, B.; Gerome, F.; Benabid, F.; Chiang, K.; Xiao, L. Ultralow-loss fusion splicing between negative curvature hollow-core fibers and conventional SMFs with a reverse-tapering method. *Opt. Express* **2021**, *29*, 22470. [CrossRef] [PubMed]